providing us the SYBYL® program.

## References

1. Cramer III, R. D.; Patterson, D. E.; Bunce, J. D. *J. Am. Chem. Soc.* **1988**, *110*, 5959.
2. (a) Horwitz, J. P.; Massova, I.; Wiese, T. E.; Wozniak, A. J.; Corbett, T. H.; Sebolt-Leopold, J. S.; Capps, D. B.; Leopold, W. R. *J. Med. Chem.* **1993**, *36*, 3511. (b) Klebe, G.; Abraham, U. *J. Med. Chem.* **1993**, *36*, 70. (c) McFarland, J. W. *J. Med. Chem.* **1992**, *35*, 2543. (d) Kim, K. H. *Med. Chem. Res.* **1991**, *1*, 259.
3. Kim, K. H.; Martin, Y. C. *J. Org. Chem.* **1991**, *56*, 2723.
4. Kim, K. H.; Martin, Y. C. *J. Med. Chem.* **1991**, *34*, 2056.
5. Yoo, S. E.; Cha, O. J. *Bull. Korean Chem. Soc.* **1994**, *15*, 889.
6. (a) Carroll, F. I.; Gao, Y.; Rahman, M. A.; Abraham, P.; Parham, K.; Lewin, A. H.; Boja, J. W.; Kuhar, M. J. *J. Med. Chem.* **1991**, *34*, 2719. (b) Waller, C. L.; McKinney, J. D. *J. Med. Chem.* **1992**, *35*, 3660.
7. Rauls, D. O.; Baker, J. K. *J. Med. Chem.* **1979**, *22*, 81.
8. Altomare, C.; Tsai, R.-S.; Tayar, N. El; Testa, B.; Carroti, A.; Cellamare, S.; De Benedetti, P. G. *J. Pharm. Pharmacol.* **1991**, *43*, 191.
9. Dennis, E. S.; John, R. V.; Robert, M. K.; Tomas, De P. *J. Pharm. Sci.* **1994**, *83*, 305.
10. Tripos Associates, 1699 S. Hanley Road, Suite 303, St. Louis, MO 63144.
11. Gasteiger, J.; Marsili, M. *Tetrahedron* **1980**, *36*, 3219.
12. Wold, S.; Ruhe, A.; Wold, H.; Dunn, W. J. *SIAM J. Sci. Stat. Comp.* **1984**, *5*, 735.
13. Cramer, R. D.; Bunce, J. D.; Patterson, D. E.; Frank, I. E. *Quant. Struct.-Act. Relat.* **1988**, *7*, 18.

# Analysis of Binodal Structures of Final State Distributions in Vibrational Predissociations of Triatomic van der Waals Molecules

**Chun-Woo Lee**

*Department of Chemistry, Ajou University, 5 Wonchun Dong, Suwon 441-749, Korea*
*Received August 18, 1995*

In this work, we focused on the setup of the tools for the analysis of the final rotational state distribution of photofragments in vibrational predissociations of triatomic van der Waals molecules A-$B_2$. We found that reflection principle used for the direct photodissociation processes can also be applied to find out the final rotational state distributions for indirect photodissociation processes. The quantity which represents the strength of rovibrational coupling between the quasi-bound state and the final state is reflected into the mirror of the classical angular momentum function, instead of the initial state before light absorption used in the reflection principle of direct processes. The sign change in the first derivative of the interaction potential with respect to the bond distance of $B_2$ is found to be the source of the binodal structures in the final rotational distributions of photofragments in the model system studied in this work. In MQDT analysis, short range eigenchannel basis functions were found to be localized in angle, in the previous work [Lee, C.W. *Bull. Korean Chem. Soc.* **1995**, *16*, 957.] and may be called angle functions. Angle functions enjoy simple geometrical structures which have simple functional relations with the final state distributions of photofragments. Two processes take place along the angle functions which resemble the quasi-bound state and dominate over other processes. Two such angle functions are found to be not only localized angularly but also localized either one of ends of $B_2$ in motions along the bond of $B_2$. These dominating photodissociation processes, however, cancel each other. This cancellation causes photodissociation to depend sensitively on the interaction potential at other angles than the dominant one. Part of potential surface where much larger torque exists can now play an important role in photodissociation. MQDT also enables us to see which processes play important roles after cancellation. This is done by examining the amounts of time delayed by asymptotic eigenchannels.

## Introduction

It is a fundamental question in chemistry how and how fast the energies deposited into molecules by lights or by collisions redistribute inside the molecules and break up chemical bonds. The investigation of such nonradiative decay processes of excited states for medium-sized molecules is, however, greatly hampered by the presence of a lot of vibrotational or electronic channels involved. It has been recognized that van der Waals molecules provide the tractable system for state-to-state studies of intramolecular energy redistributions.[1] Van der Waals bonds are so weak that even one quantum excitation of vibration motion is in many cases enough to break down the bond without exciting electronic states. Consequently the number of channels involved are greatly reduced in the predissociation of van der Waals mol-

ecules. Besides such tractability and simplification, the study of predissociation mechanism of van der Waals molecules provides several useful applications. Unexpectively large low energy collision-induced vibrational relaxations may be understood from the van der Waals predissociation mechanism. Energy transfers in solids most probably take place with the same mechanism.

For this reason, a lot of theoretical and experimental work on the predissociation of van der Waals molecules have been done and reviewed by many authors.[1] Nevertheless, we have reasons to study this system. For direct photodissociation processes, reflection principles provide convenient tools, as greatly emphasized by Schinke,[2] for understanding the general shapes of absorption spectra or of final quantum number distributions of photofragments. According to the reflection principles, observables like dissociation spectra or final state distributions reflect the shapes of the molecular wavefunctions before light absorption. The reflections are done on the mirrors whose shapes are determined by the so called classical excitation functions of the conjugate variables to observables. For the indirect processes, however, reflections of wavefunctions before light absorption into the final state distributions can not be done as photodissociation processes pass some quasi-bound states. Thus we need other tools to investigate the photodissociation dynamics around resonances. In devising such tools, we have to deal with the difficulties caused by the fact that observables such as the partial photodissociation cross sections and asymmetric parameters undergo dramatic changes around resonances.

Indirect photodissociation may be studied by assuming the presence of quasi-bound states and then by considering their configuration interactions with continua as considered by Fano.[3] By this way, Fano was able to get the analytical solutions and showed that the total photodissociation cross section can be described by a simple Fano-Beutler formula. The formula contains only four parameters, *i.e.* photodissociation cross section at off-resonance (background), resonance energy, lifetime, and line profile index. He could show that asymmetric shapes, often seen in photoionization spectra, derives from the interferences between resonance and principal contributions. Unfortunately, he only obtained the total photodissociation cross sections. Combet-Farnoux and I independently derived the formula for the partial photodissociation cross section which has the identical form with the Fano-Beutler one except for the line profile index which is now a complex number in general.[4] Since the analytical form of photodissociation cross section around a resonance was obtained, we could tell what parameters and which combinations of them are responsible for the observables. Using this analytical solution, the theoretical basis was given in Ref. 4 for the Golden-rule like expression which is known to be good for the treatment of predissociating system of van der Waals molecules. In the Golden-rule like expression, final state distributions after photodissociation do not depend on the wavefunctions before light absorption. They are determined by the coupling between quasi-bound states and final states *via* interaction potentials. This Golden-rule like formula is one of the starting point of devising the tools for the analysis of predissociation dynamics. Section 3 will show that a kind of rotational reflection principle similar to that in the direct photodissociation may also be applied for obtaining the final rotational state distributions when an infinite order sudden approximation (IOS) is applied for the final state in the Golden-rule like formula.

Though Fano's configuration interaction theory yields an analytical solution on photodissociation processes, it has fundamental drawbacks. From the outset, it assumes the existence of a quasi-bound state as a separate thing from the continua. Theoretically, there is no fundamental difference between continuum and bound states. Wavefunctions of motions along some channels become bound and continuum states as the energies of motions become negative and positive, respectively. This view of bound states as being produced by the closed channels is simpler than that of configuration interaction theory in that bound and continuum states are treated on the same footing. Then interactions between bound and continuum wavefunctions in the configuration interaction theory are replaced by the channel interactions between closed and open channels. Usually, as a closed channel contains a series of bound states like a Rydberg series, treating the interactions between a series of bound states and a continuum by a channel interaction between a closed and an open channel provides simpler theoretical framework.

Such a view of seeing interactions between bound states and continua as the ones among channels and seeing the existence of bound states as derived from the existence of closed channels were implemented as the multichannel quantum defect theory by Seaton.[5] Fano realized that channel interactions which are very complicated in nature occur mostly in the small region of space and affect the observables in the asymptotic region only through the eigenphases of eigenchannel states in the inner small region (called short-range eigenchannel states by him). Then he could identify small numbers of parameters which are characteristics of channel interactions and which vary slowly as functions of energy. Such small numbers of parameters yield the complicated spectra as functions of energy around resonances when boundary conditions at the asymptotic region are applied and some channels become closed.

In the previous papers, successful implementation of MQDT to the inelastic scattering and predissociation of triatomic van der Waals molecules was reported.[6] In this work, MQDT will be used as a tool for investigating predissociation dynamics of triatomic van der Waals molecules. Section 4 shows how to use MQDT to examine further in detail what is going on during the vibrational predissociation of van der Waals predissociation.

Though the purpose of this paper is to develop rather general analytic tools for predissociation dynamics, particular attention will be paid on the analysis of the binodal structure observed in experiments with the model potential. Analysis based on the real potential will be deferred for the future work.

## System

The system used here is the same as the one used in Ref. 6. Let us describe it briefly. The system is the one of the vibrational predissociation of triatomic van der Waals molecules. Triatomic van der Waals molecules are restricted to rare gas-homonuclear halogen diatomic molecules. Empirical potentials for them like $NeCl_2$, $HeCl_2$[7] are well established

owing to the state-to-state measurements available for them. The interaction potential between A and $B_2$ in $AB_2$ triatomic system used by Halberstadt *et al.*[8] for $NeCl_2$ system has the following form (a slightly modified form for $HeCl_2$)

$$V(R,r,\gamma)=V_M(R,r,\gamma), \text{ when } R\le R^*,$$

$$V(R,r,\gamma)=V_{vdW}(r,\gamma)+(V_M-V_{vdW})e^{-\rho\left(\frac{R-R^*}{R^*}\right)^2}, \text{ when } R\ge R^*, \quad (1)$$

in the Jacobi coordinates $R$, $r$, $\gamma$ that denote the distance between A and the center of mass of $B_2$, the bond distance of $B_2$, and the angle between $\vec{R}$ and $\vec{r}$, respectively. $V_M(R,r,\gamma)$ and $V_{vdW}$ are given as

$$V_M(R,r,\gamma)=D_{AB}\sum_{i=1}^{2}\{[e^{-\alpha_{AB}(R_{AB_i}-R_{AB}^{(e)})}-1]^2-1\}^2 \quad (2)$$

$$+D_{CM}\{[e^{-\alpha_{CM}(R-R_{CM}^{(e)})}-1]^2-1\}^2, \quad (3)$$

$$V_{vdW}(R,\gamma)=-\frac{C_6(\gamma)}{R^6}-\frac{C_8(\gamma)}{R^8}, \quad (4)$$

where $R_{AB_i}$ is the distance between A and $i^{th}$ B atom, $R$ is the same as above, and other parameters are constant that are adjusted to yield the best fit to the experimental values. Two Legendre terms are retained for $C_6(\gamma)$ and $C_8(\gamma)$, e.g.,

$$C_6(\gamma)=C_{60}+C_{62}P_2(\cos\gamma). \quad (5)$$

$R^*$ is chosen as the inflection point of the atom-atom Morse potentials and given by $R^*=R_{CM}^{(e)}+\ln 2/\alpha_{CM}$. The parameters used in this paper are the same as those of Ref. 6 and repeatedly given here in Table I for self-completeness.

With this interaction potential, the Hamiltonian for the triatomic van der Waals molecules $AB_2$ is given in the Jacobi coordinates by[9]

$$H=-\frac{1}{2m}\frac{\partial^2}{\partial R^2}+\frac{\vec{j}^2}{2\mu r^2}+\frac{\vec{l}^2}{2mR^2}+V(R,r,\gamma)+H_{B_2}(r), \quad (6)$$

with

$$H_{B_2}(r)=-\frac{1}{2\mu r^2}\frac{\partial^2}{\partial r^2}+V_{B_2}(r), \quad (7)$$

that denotes the vibrational Hamiltonian of $B_2$. $m$ and $\mu$ denote the reduced mass of A and the center of mass of $B_2$ and of $B_2$, respectively; $\vec{j}$, the angular momentum operator of $B_2$; and $\vec{l}$, the orbital angular momentum operator of the relative motion of A and the center of mass of $B_2$.

The values of total angular momentum operator $\vec{J}=\vec{j}+\vec{l}$, as is well known both experimentally and theoretically, do not affect the predissociation dynamics much and is set to zero hereafter. This simplifies the Hamiltonian as $\vec{l}$ can be set to being equal $\vec{j}$.

When the wavefunctions $\Psi^{-(i)}(R,r,\gamma)$ to the dissociation channel $i=\{vj\}$ are expanded in base functions $\Phi_{i'}(r,\gamma)=(r|v)Y_{j_0}(\gamma,0)$ for the rovibrational channel $i'=\{v'k'\}$ as

$$\Psi_i(R,r,\gamma)=\sum_{i'}\Phi_{i'}(r,\gamma)\chi_{i'i}(R), \quad (8)$$

the close-coupling equations are given as

$$\left[-\frac{1}{2m}\frac{d^2}{dR^2}-k_{i'}^2+\frac{\vec{j}}{2mR^2}\right]\chi_{i'i}(R)+\sum_{i''}V_{i'i''}(R)\chi_{i''i}(R)=0, \quad (9)$$

with

$$k_i^2=2m[E-Bj(j+1)-(v+\frac{1}{2})\omega], \quad (10)$$

and

$$V_{i''i'}(R)=\int d\gamma\ \sin\gamma\int dr\Phi_{i''}(r,\gamma)V(R,r,\gamma)\Phi_{i'}^*(r,\gamma). \quad (11)$$

In the practical calculations of $V_{i''i'}(R)$, the interaction potential is expanded into Legendre polynomials and then the angle integration is performed analytically to yield the formula in terms of 3j symbols.

The real symmetric $K$ matrix in Eq. (26) is easily obtained by simply replacing $\exp(\pm ik_iR)$ or $\sin k_iR$ and $\cos k_iR$ in the conventional close-coupling computer code with the energy normalized base pair $f_i(R)$ and $g_i(R)$. The important difference between the close-coupling and the $K$ matrix calculation is that the subindex $i$ includes both open and closed channels for the latter while only open channels for the former.

## Analysis of rotational state distribution by IOS

Infinite order sudden approximation (IOS)[10] assumes photodissociation processes to take place at fixed angles $\gamma$. In our problem, we apply IOS to the final state wavefunction in the Golden-rule like formula which is known to be applicable for the predissociations of van der Waals molecules.[1,4] In the Golden-rule like formula, partial photodissociation cross sections $\sigma_{nj}$ to the dissociation channels $\{nj\}$ are assumed to be proportional to

$$\sigma_{nj}\propto 2\pi|(\phi_b|V|\Psi_c^{-(nj)})|^2. \quad (12)$$

$\Psi_c^{-(nj)}$ are approximately obtained by IOS method. If we consider the continuum wavefunctions without closed channel contributions, or without $n=1$ channel contributions, IOS continuum wavefunctions satisfy the following ordinary differential equations

$$\left[-\frac{1}{2m}\frac{\partial^2}{\partial R^2}+\frac{l^2}{2\mu R^2}+Bj^2+E_{n=0}+V_0(R,\gamma)\right]\Psi^{IOS}(R|\gamma)$$
$$=E\Psi^{IOS}(R|\gamma), \quad (13)$$

where $E_{n=0}$ is the vibrational energy of the diatomic molecule when its vibrational quantum number is zero. As mentioned earlier, $J=0$ was assumed and $j$ and $l$ have identical values of, let us say, $j_0$. That is, $j^2=l^2=j_0(j_0+1)$ where $j_0$ is an arbitrary positive integer. The exact value of $j_0$ is not important. The reason for that may be easily understood if a IOS wavefunction is understood as a wavefunction at the short-range where the potential is highly negative and the rotational energy is much smaller than the kinetic energy of the relative motion along the dissociative coordinate $R$. IOS wavefunction $\Psi^{IOS}$ satisfies an incoming wave boundary condition

$$\Psi^{IOS}(R|\gamma)\to k_0^{-1/2}[e^{ik_0R}+S_0e^{-ik_0R}]$$
$$\to 2k_0^{-1/2}e^{-i\eta(\gamma)}\cos[k_0R+\eta(\gamma)], \text{ as } R\to\infty, \quad (14)$$

where $\eta$ is the phase shift at the given angle $\gamma$.

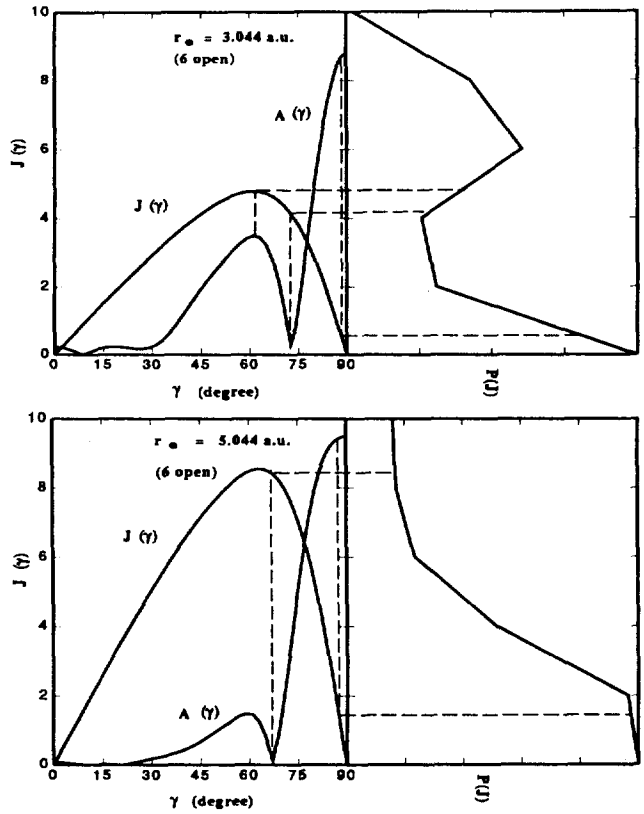


**Figure 1.** The diagrams showing rotational reflection principle for the Golden-rule like expressions where continuum functions are treated with IOS approximation

With this IOS wavefunction, $\Psi_c^{-(0)}(R,r,\gamma)$ may be obtained as

$$\Psi_c^{-(0)}(R,r,\gamma)=\Psi_c^{-(0)}(R,\gamma)<r|0>=\Psi^{IOS}(R|\gamma)Y_{j0}(\gamma,0)<r|0>, \quad (15)$$

as can be confirmed by the examination of the boundary conditions they satisfy

$$\begin{aligned}Y_{j0}(\gamma,0)\Psi^{IOS}(R|\gamma)&\rightarrow k_j^{-1/2}[e^{ik_jR}Y_{j0}(\gamma,0)+e^{-k_jR}Y_{j0}(\gamma,0)S_j^{IOS}(\gamma)]\\&\rightarrow k_j^{-1/2}[e^{ik_jR}Y_{j0}(\gamma,0)+\sum_{j'}Y_{j'0}(\gamma,0)S_{j'j}^{IOS}e^{-ik_jR}]\\&\rightarrow\sum_{j'}Y_{j'0}(\gamma,0)\{k_{j'}^{-1/2}[e^{ik_{j'}R}\delta_{j'j}+S_{j'j}^{IOS}e^{-ik_{j'}R}]\}\\&=\Psi^{-(j)}(R,\gamma). \quad (16)\end{aligned}$$

Then

$$\begin{aligned}(\phi_b|V|\Psi_c^{-(0j)})&\approx(\phi_b|V|Y_{j0}\Psi^{IOS})|n=0>\\&\approx<1|r-r_e|0>2\pi\int_0^\pi d\gamma\sin\gamma Y_{j0}(\gamma,0)A(\gamma)e^{i\eta(\gamma)}, \quad (17)\end{aligned}$$

where $A(\gamma)$ is the modulus of the following integral,

$$\begin{aligned}A(\gamma)\exp[i\eta(\gamma)]&=\int_0^\infty dR\Phi_b(R,r)\left[\frac{\partial V}{\partial r}\right]_{r=r_e}\Psi^{IOS}(R|\gamma)\\&=\int dR\sum_{j'}Y_{j'0}(\gamma,0)\chi_{bj'}(R)\left[\frac{\partial V}{\partial r}\right]_{r=r_e}\Psi^{IOS}(R|\gamma). \quad (18)\end{aligned}$$

The $\eta(\gamma)$ in Eq. (18) is the phase of the IOS wavefunction $\Psi^{IOS}(R|\gamma)$:

$$\Psi^{IOS}(R|\gamma)=|\Psi^{IOS}(R|\gamma)|\exp[i\eta(\gamma)]. \quad (19)$$

$J(\gamma)$ is shown in Figure 1. The figure shows that $A(\gamma)$ is zero at $\gamma=0$ and $\pi/2$ where the phase shifts of the IOS function $\Psi^{IOS}(R|\gamma)$ are symmetric and their first derivatives with respect to $\gamma$ become zero. $A(\gamma)$ has a maximum at 72° for $r_e=3.044$ a.u. If we apply a semiclassical approximation to the spherical harmonics,[9]

$$\begin{aligned}Y_{j0}(\gamma,0)&\approx\sqrt{\frac{2(2j+1)}{4\pi^2 j\sin\gamma}}\cos\left[\left(j+\frac{1}{2}\right)\gamma-\frac{\pi}{4}\right]\\&\sim\frac{1}{2}\pi^{-1}\sin^{-1}\gamma\left(\exp\left\{i\left[\left(j+\frac{1}{2}\right)\gamma-\frac{\pi}{4}\right]\right\}\right.\\&\left.+\exp\left\{-i\left[\left(j+\frac{1}{2}\right)\gamma-\frac{\pi}{4}\right]\right\}\right), \quad (20)\end{aligned}$$

the integral appearing in Eq. (17), which will be denoted as $I$, may be approximated as

$$\begin{aligned}I=\frac{1}{2}\pi^{-1}\int_0^\pi d\gamma\sin^{1/2}\gamma A(\gamma)&\left(\exp\left\{i\left[\left(j+\frac{1}{2}\right)\gamma-\frac{\pi}{4}+\eta\right]\right\}\right.\\&\left.+\exp\left\{i\left[\eta-\left(j+\frac{1}{2}\right)\gamma+\frac{\pi}{4}\right]\right\}\right). \quad (21)\end{aligned}$$

According to a semiclassical theory, the first derivative of $\eta(\gamma)$ with respect to $\gamma$ is the classical angular momentum function and will be denoted by $J(\gamma)$. Applying the steep decent method, Eq. (21) becomes

$$\begin{aligned}I\sim\frac{1}{2}\pi^{-1}&\left(\exp\left\{i\left[\eta(\gamma_1)-\left(j+\frac{1}{2}\right)\gamma_1\right]\right\}\sin^{1/2}\gamma_1 A(\gamma_1)\left[\frac{\sqrt{2\pi}}{\left(\frac{\partial J}{\partial\gamma}\right)_{\gamma_1}}\right]^{1/2}\right.\\&\left.+\exp\left\{i\left[\eta(\gamma_2)-\left(j+\frac{1}{2}\right)\gamma_2\right]\right\}\sin^{1/2}\gamma_1 A(\gamma_2)\left[\frac{\sqrt{2\pi}}{\left(\frac{\partial J}{\partial\gamma}\right)_{\gamma_2}}\right]^{1/2}\right). \quad (22)\end{aligned}$$

The above equation tells us that the integral becomes larger as $A(\gamma)$ and the inverse of the first derivative of the classical angular momentum function with respect to angle $\gamma$ are larger. The geometrical visualization of this is just the reflection principle. Let us consider the overlapped graphs of the classical angular momentum $J(\gamma)$ and $A(\gamma)$ as functions of angle $\gamma$ as shown in Figure 1. At a given angle $\gamma$, say $\gamma_0$, let us draw a perpendicular line upward from the point $[\gamma_0, A(\gamma_0)]$ to the point $[\gamma_0, J(\gamma_0)]$ and from there draw the horizontal line rightward to produce a curve of a rotational distribution in the diatomic photofragment, *i.e.* $P(J)$ *vs.* $J$, as shown in Figure 1. According to the semiclassical theory, rotational quantum number $j$ differ from rotational excitation function $J(\gamma)$ by 1/2, *i.e.* $j+1/2=J(\gamma)$. Since rotational reflection principle based on Eq. (21) is a rough theory, $j\approx J(\gamma)$ is employed in Figure 1. The figure tells us that the rotational quantum number distribution reflects the shape of $A(\gamma)$ with the mirror given by the classical angular momentum function.

Now let us find out, from the viewpoint of the IOS approximation, the explanation for the fact that a binodal structure is shown up when $r_e=3.044$ a.u. while it does not when $r_e=5.044$ a.u.. Figure 1 compares two graphs of $J(\gamma)$ *vs.* $\gamma$ corresponding to the cases of $r_e=3.044$ and 5.044 a.u.. Two graphs have different maximum values. The $r_e=5.044$ a.u. case has a bigger maximum value of $A(\gamma)$ owing to the bigger anisotropy felt by A from $B_2$ at the same value of $R$ comparing to the $r_e=3.044$ a.u. case. Since the classical angular momen-

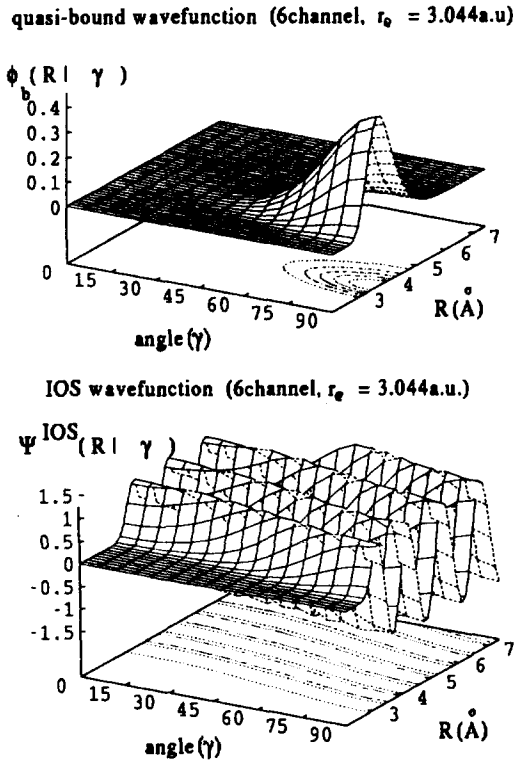


**Figure 2.** The quasi-bound wavefunction and the IOS wavefunction obtained by including 6 closed channels when $r_e$=3.044 a.u.

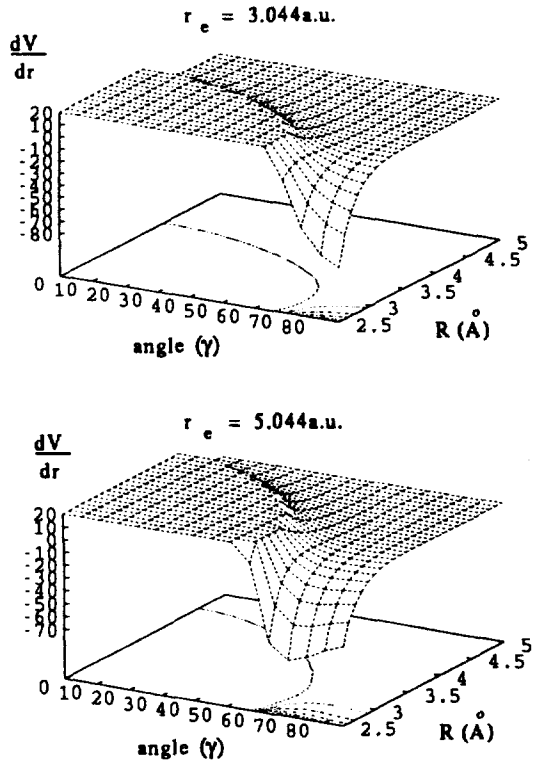


**Figure 3.** $(dV/dr)_{r_e}$ *vs.* angle and $R$.

tum function $J(\gamma)$ is the first derivative of $\eta(\gamma)$ with respect to $\gamma$ and $\eta(\gamma)$ may be written in phase amplitude method as

$$\eta(\gamma)=-\frac{2}{k}\int_0^\infty V_0(R,\gamma)\left[\Psi^{IOS}(R|\gamma)\right]^2\,dR, \tag{23}$$

$J(\gamma)$ may be written as

$$J(\gamma)=-\frac{2}{k}\left\{\int_0^\infty \frac{\partial V_0(R,\gamma)}{\partial\gamma}\,[\Psi^{IOS}(R|\gamma)]^2 dR + \int_0^\infty V_0(R,\gamma)\frac{\partial[\Psi^{IOS}(R|\gamma)]^2}{\partial\gamma}\,dR\right\}. \tag{24}$$

According to Figure 2, $\Psi^{IOS}(r|\gamma)$ is a slowly varying function of $\gamma$ and the second term in Eq. (24) may be neglected comparing to the first term. Since $-(\partial V_0(R,\gamma)/\partial\gamma)$ is the torque, the above equation tells us that, the bigger the torque is, the bigger the classical angular momentum function is, conforming to the common sense. Classical angular momentum function shown in Figure 1 tells us that the maximum torque occurs at angles around 60°, where anisotropy of the potential is the biggest.

Besides that, two graphs are similar in that $J(\gamma)$ equal zeros at 0 and 90° and have maxima around 60°. Figure 1 also shows the graphs of $|A(\gamma)|$ *vs.* $\gamma$. $A(\gamma)$ changes sign at $\gamma\approx73°$ for $r_e$=3.044 a.u. while at $\gamma\approx67°$ for $r_e$=5.044 a.u.. Because of this difference in angles of sign changes, the maximum of $J(\gamma)$ almost coincides with the second maximum of $A(\gamma)$ for $r_e$=3.044 a.u. while it lies more close to the zero of $A(\gamma)$ for $r_e$=5.044 a.u.. Therefore, whether binodal structures are shown up or not is determined by the relative position of the zero of $A(\gamma)$ and the maximum of $J(\gamma)$.

Next let us examine what brings about the differences in values of angle $\gamma$ where magnitudes of $A(\gamma)$ are equal to zeros. $A(\gamma)$ is given by Eq. 18 and its magnitude is determined by the behaviors of three functions, quasi-bound state wavefunctions $\phi_b(R,\gamma)$, continuum wavefunctions $\Psi^{IOS}(R|\gamma)$ and $[\partial V/\partial r]_{r_e}$. Two graphs, $\phi_b(R,\gamma)$ and $\Psi^{IOS}(R|\gamma)$ *vs.* $R$ and $\gamma$ when $r_e$=3.044 a.u, are shown in Figure 2. Corresponding graphs for $r_e$=5.044 a.u. are similar to those for $r_e$=3.044 a.u. and are not shown. Figure 3 shows $[\partial V/\partial r]_{r=r_e}$ for both cases. The figure shows that $[\partial V/\partial r]_{r=r_e}$ changes its sign at $\gamma$ around 57° in case of $r_e$=5.044 a.u. while at near 68° in case of $r_e$=3.044 a.u.. The reason why the angle of sign change is smaller in the former may be ascribed to the relatively larger values of $r_e$ in that case.

In order to understand this, let us first understand why and how the sign of the torque changes as a function of angle $\gamma$. In order to be more specific, let us choose the value of $R$ as 2.5 Å. The other choice of $R$ may give similar results. At $R$=2.5 Å and $\gamma$=90°, the distances between A and each of atoms of $B_2$ are smaller than 3.5-3.6 Å where the minima of Morse potentials take place when the intermolecular potential parameters are given by Table 1. Then the increase of the diatomic distance $r$ makes the distances between A and $B_2$ larger and closer to 3.5-3.6 Å and makes the magnitudes of intermolecular potential smaller. Since the magnitude of intermolecular potential becomes smaller as $r$ increases, the sign of $[\partial V/\partial r]_{r=r_e}$ is negative. But the increase of diatomic distance $r$ does not always lead to the increase of the distance between A and $B_2$. At $\gamma$ smaller than a cos($r$/2 $R$), the increase of $r$ leads to the decrease of the distance between A and $B_2$ and thus increase the magnitude of the

**Table 1.** Values of potential parameters used in this paper

| | |
|---|---|
| (a) Reduced mass between A and $B_2$ | |
| m=6756.8 a.u. | |
| (b) Morse potential parameter | |
| $D_{AB}$=0.0034 eV | $D_{CM}$=0.00195 eV |
| $\alpha_{AB}$=1.0 a.u.$^{-1}$ | $\alpha_{CM}$=1.0 a.u.$^{-1}$ |
| $R_{AB}^{(e)}$=6.82 a.u. | $R_{CM}^{(e)}$=6.65 a.u. |
| (c) van der Waals potential parameter | |
| $C_{60}$=0.75 eV (a.u.)$^{-6}$ | |
| $C_{62}$=0.119 eV (a.u.)$^{-6}$ | |
| $C_{80}$=1.58 eV (a.u.)$^{-8}$ | |
| $C_{82}$=0.8 eV (a.u.)$^{-8}$ | |
| (d) Diatomic molecular parameters | |
| $\omega_e$ | 0.0162 eV |
| $B$ | 0.01758 meV |
| $r_e$ | 3.044 a.u. |
| $\mu$ | 32576.6 a.u. |

intermolecular potential. The magnitude of angle $\gamma$ of sign change, then, becomes smaller as $r$ becomes larger.

The momentum gap law[1] can be understood from the very form of $A(\gamma)$. In Eq. 18, as the relative energy becomes bigger, $\Psi^{IOS}(R|\gamma)$ oscillates more and then the integral will become smaller.

## Analysis of rotational state distribution by MQDT

**Brief summary of MQDT.** Infinite order sudden approximation decouples the motions among different angles $\gamma$ and allows us to treat the motion along the dissociation coordinate $R$ as an elastic process. The knowledge on the behavior of the elastic phase shift $\eta(\gamma)$ as a function of $\gamma$ and the application of the semiclassical theory by Ford and Wheeler[9] to the Golden rule like expression for the partial photodissociation cross section enable us to understand the predissociation dynamics by a sort of reflection principle. Though IOS approximation is a powerful tool for the purpose of interpretation of the predissociation dynamics, it has several defects, as mentioned in Section 1.

MQDT has no such defects as IOS has. It is in principle as exact as close-coupling method is. Its interpretational power surpasses that of IOS approximation in many respects. But they share the same principle. Namely, they realize, at least implicitly, that most photodissociation dynamics occur at inner or short-range region. The IOS wavefunction obtained by solving Eq. (13) at fixed $\gamma$ may be considered as channel wavefunctions at the short-range.

Since MQDT was described elsewhere, let us summarize only relevant stuff here. In MQDT, coordinates $R$ along which fragmentation takes place are divided into two regions $R \le R_0$ and $R > R_0$. The matching radius $R_0$ where log derivatives of the solutions at the inner and outer regions coincide, is usually taken so that all inelastic processes are included in the inner region. In the outer space, motions in the different channel states are decoupled. If standing wave channel basis functions $\Psi_{i'}$ are considered, their radial wave functions denoted by $\chi_{ii'}(R)$ for the $i$ channel state $\Phi_i$

$$\Psi_{i'}=\sum_i \Phi_i(\omega)\chi_{ii'}(R), \tag{25}$$

obey the ordinary second order differential equations and are given as linear combinations of regular and irregular solutions

$$\Psi_{i'}(R,\omega)=\sum_i \Phi_i(\omega)[f_i(R)\delta_{ii'}-g_i(R)K_{ii'}],\ R \ge R_0, \tag{26}$$

where $\omega$ denotes collectively all the coordinates but $R$ and $K_{ii'}$ is the real symmetric matrix which differs from the usual $K$ matrix in that its indices $i$ and $i'$ run over not only open but also closed channels. The eigenvalues of $K$ matrix are conveniently parameterized as $\pi\mu_\alpha$ where $\mu_\alpha$ (or $\pi\mu_\alpha$) are called eigenquantum defects (or eigenphaseshifts).[11] If we denote the matrix made of eigenvectors of $K$ as $U$, energy normalized short-range eigenchannel basis functions are given by

$$\Psi_\alpha=\sum_i \Psi_i U_{i\alpha} \cos \pi\mu_\alpha$$
$$=\sum_i \Phi_i(\omega)U_{i\alpha}[f_i(R)\cos \pi\mu_\alpha - g_i(R)\sin \pi\mu_\alpha]. \tag{27}$$

$\Psi_i$ and $\Psi_\alpha$ are not suitable for the description of the asymptotic region. We may now consider eigenchannel basis functions $\Psi_\rho$ at the asymptotic region, which are eigenvectors of $S$ matrix or $K$ matrix at the asymptotic region. $\Psi_\rho$ may be obtained as superpositions of $\Psi_\alpha$

$$\Psi_\rho=\sum_\alpha \Psi_\alpha A_{\alpha\rho}. \tag{28}$$

In order to satisfy boundary conditions at the asymptotic region, $A_{\alpha\rho}$ should satisfy the following equations

$$\sum_\alpha U_{i\alpha}\sin(\beta_i+\pi\mu_\alpha)A_{\alpha\rho}=0,\ i \in \text{closed}, \tag{29}$$

$$\sum_{i\alpha} U_{i\alpha}\cos \pi\mu_\alpha A_{\alpha\rho}=T_{i\rho}\cos\pi\tau_\rho,$$
$$\sum_{i\alpha} U_{i\alpha}\sin\pi\mu_\alpha A_{\alpha\rho}=T_{i\rho}\sin\pi\tau_\rho,\ i \in \text{open}. \tag{30}$$

$\Psi^{-(i)}$, satisfying the incoming wave boundary conditions, are obtained as linear combinations of $\Psi_\alpha$

$$\Psi^{-(i)}=\sum_\alpha A_\alpha{}^{-(i)}\Psi_\alpha, \tag{31}$$

with

$$A_\alpha{}^{-(i)}=ie^{-i\eta_i}\sum_\beta U_{i\beta}e^{-i\pi\mu_\beta}\Delta_{\beta\alpha}. \tag{32}$$

Instead of $A_\alpha{}^{-(i)}$, it may be more convenient to use $B_\alpha{}^{-(i)}$ which are defined as

$$B_\alpha{}^{-(i)}=\sum_\beta U_{i\beta}e^{-i\pi\mu_\beta}\Delta_{\beta\alpha}. \tag{33}$$

Transition dipole moments $D^{-(i)}$ are expressed as a linear combination of energy insensitive transition moments $D_\alpha=(\Psi_\alpha|\mu|\Psi_{gr})$ to the short-range eigenchannels $\Psi_\alpha$:

$$|D^{-(i)}|=\left|\sum_\alpha B_\alpha{}^{-(i)}D_\alpha\right|. \tag{34}$$

**MQDT version of Golden-rule like formula.** Let us now analyze Eq. (34). From the outset, we anticipate that values of $\Delta_{\alpha\beta}$ will be larger as $\alpha$ and $\beta$ channel wave functions resemble $\Psi_{gr}$ by Planck-Condon principle. Calculation

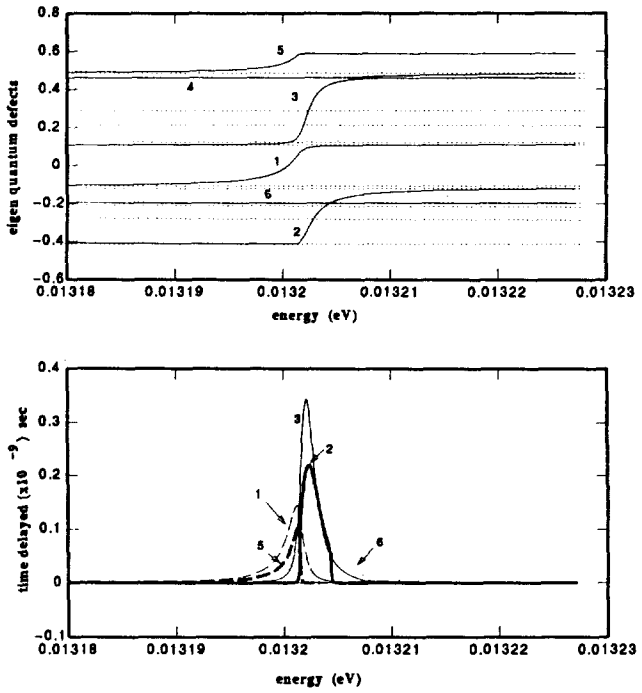


**Figure 4.** Eigenquantum defects $\mu_\alpha$ and $\tau_\rho$ calculated around the resonance energy 0.0132026 eV with 12 channels (6 open, 6 closed) and with $r_e$=3.044 a.u. are shown in the first graph. $\tau_\rho$ are drawn by solid lines while $\mu_\alpha$ are drawn by dashed lines. The second graph shows times delayed by resonances for each eigenchannel ρ.

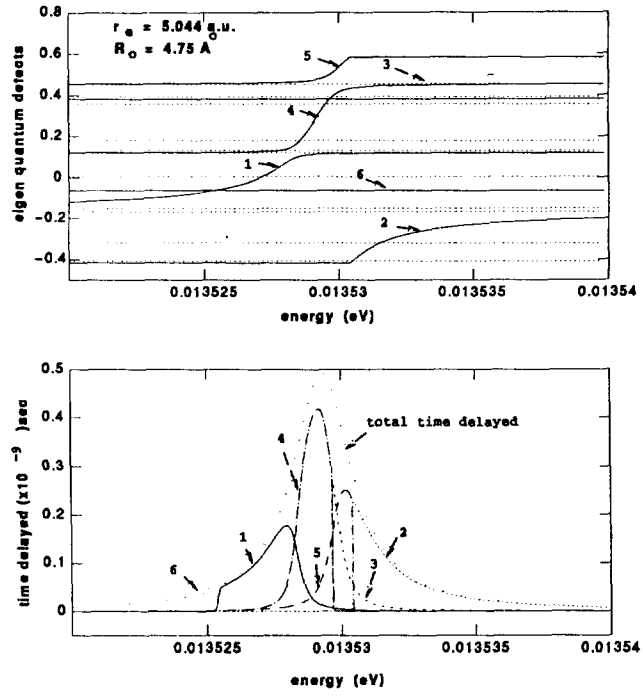


**Figure 5.** Eigenquantum defects $\mu_\alpha$ and $\tau_\rho$ calculated around the resonance energy 0.01353 eV with 12 channels (6 open, 6 closed) and with $r_e$=5.044 a.u. are shown in the first graph. $\tau_\rho$ are shown by solid lines while $\mu_\alpha$ are shown by dashed lines. The second graph shows times delayed by resonances for each eigenchannel ρ.

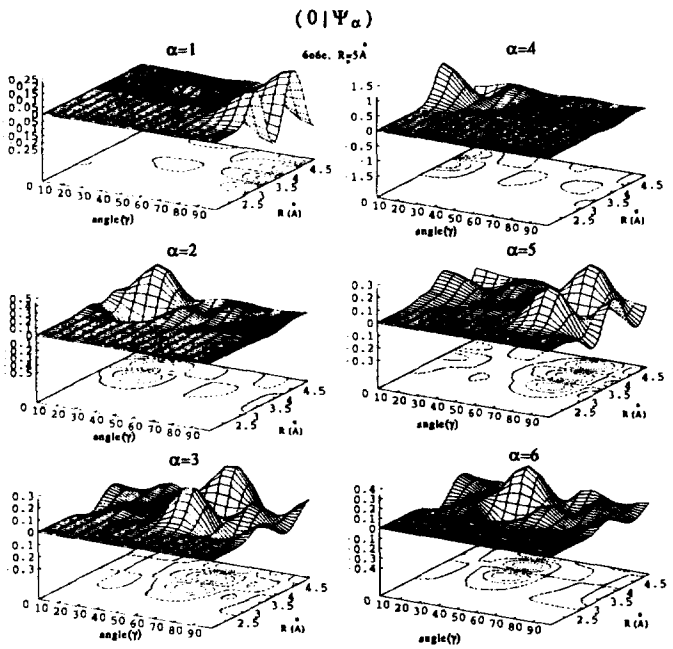


**Figure 6.** Short-range channel basis functions $\Psi_\alpha(E)$ when $r_e$= 3.044 a.u..

shows that $\Delta_{\alpha\beta}$ for $\alpha=1$ and 7, *i.e.* $\Delta_{11}$, $\Delta_{17}$, $\Delta_{77}$, dominate over other $\Delta_{\alpha\beta}$ when $r_e$=3.044 a.u. and 12 channel with 6 open and 6 closed are included. Their variations as functions of energy follow Lorentzian shapes and their magnitudes are close together. Also values of $\mu_\alpha$ for $\alpha=1$ and 7 channels are close together. This means that frame transformation matrices $U_{i\alpha}$ have comparable absolute magnitudes for two channels $\alpha=1$ and 7. By Eq. (33), $B_\alpha{}^{-(i)}$ will have similar magnitudes for $\alpha=1$ and 7. Then $D^{-(i)}$ may be approximated as

$$D^{-(i)}\approx B_1{}^{-(i)}D_1+B_7{}^{-(i)}D_7\approx B_1{}^{-(i)}(D_1+D_7), \tag{35}$$

indicating that final state distributions of photofragments only depend on $B_1{}^{-(i)}$ and not on $D_\alpha$ (or on the initial state $\Psi_{gr}$). Since $B_1{}^{-(i)}$ has to do only with the final state, transition dipole moments $D^{-(i)}$ do not depend on the initial state. Final state distributions were found to have the same characteristics in the Golden-rule like formula in configuration interaction theory. The fact that transition dipole moments $D^{-(i)}$ are approximately separable in $B_\alpha{}^{-(i)}$ and $D_\alpha$ forms the MQDT version of Golden-rule like expression in configuration interaction theory. Before discussing on the structure of $B_1{}^{-(i)}$, let us examine what are the characteristics of $\Psi_\alpha$ when $\alpha=1$ and 7.

**Characteristics and properties of short-range wavefunctions.** $\Psi_\alpha$ are obtained by linear combinations of $\Psi_i$ given as Eq. (27), which are in turn obtained by applying the boundary condition (26) on the close coupling equations. Or,

$$\Psi_\alpha=\sum_{nj}\Psi_{nj}U_{nj,\alpha}\cos\pi\mu_\alpha$$
$$=<n=1|\Psi_\alpha>+<n=0|\Psi_\alpha>, \tag{36}$$

if vib-rotational quantum numbers $\{n,j\}$ are explicitly shown for $i$ in Eq. (27). Figure 6 and 7 shows $n=1$ portion of $\Psi_\alpha$,

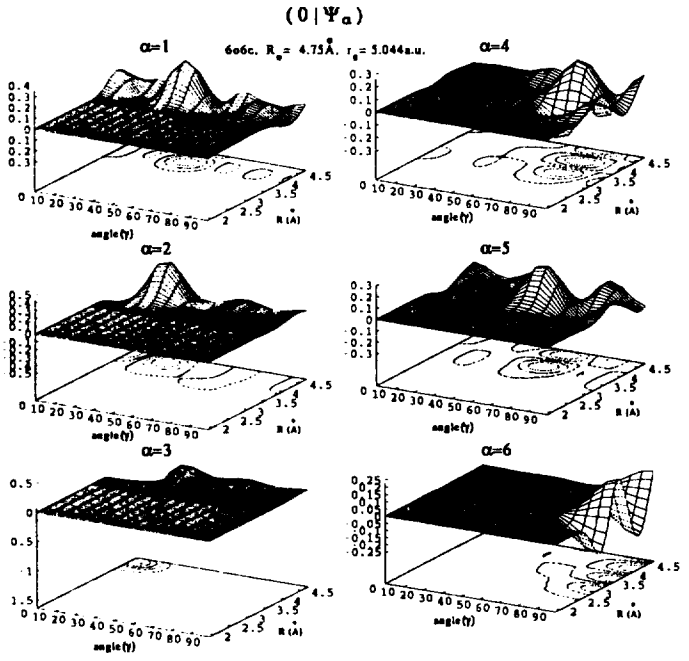


**Figure 7.** Short-range channel basis functions $\Psi_\alpha(E)$ when $r_e$= 5.044 a.u..

**Table 2.** Squares of the moduli of expansion coefficients of angle functions in terms of spherical harmonics

| $j$ | 0 | $\pi/10$ | $\pi/5$ | $3\pi/10$ | $2\pi/5$ | $\pi/2$ |
|---|---|---|---|---|---|---|
| 0 | 1.00 | 1.00 | 1.00 | 1.00 | 1.00 | 1.00 |
| 2 | 5.00 | 3.67 | 1.16 | 0.00 | 0.64 | 1.25 |
| 4 | 9.00 | 2.85 | 0.38 | 1.43 | 0.03 | 1.27 |
| 6 | 13.00 | 0.52 | 2.11 | 0.52 | 0.28 | 1.27 |
| 8 | 17.00 | 0.29 | 0.07 | 0.56 | 1.07 | 1.27 |
| 10 | 21.00 | 2.53 | 1.69 | 1.41 | 1.30 | 1.27 |

*i.e.* $<n=1|\Psi_\alpha>$, in $R$ and $\gamma$ space for $r_e$=3.044 and 5.044 a.u., respectively. The shape of the remaining $<n=0|\Psi_\alpha>$ is similar to that for $n=1$ except for having more oscillations in $R$ as the kinetic energy of the motion along $R$ is larger. Figure 6 and 7 show clearly that $\Psi_\alpha$ have magnitudes around some particular angles $\gamma$. This may be viewed as a quantum mechanical basis of the IOS approximation. The $\alpha=1$ and 7 channel basis functions $\Psi_\alpha$ have their most magnitudes around $\gamma=90°$. This rationalization of $\Psi_\alpha$ as the quantum mechanical basis of IOS approximation is already given in Ref. 6. Let us consider the geometrical implication of angle functions. If the angle function $\Psi_\alpha$ is of a Dirac type, having values only at the particular angle $\gamma_0$, and if we consider a photodissociation process taking place along the eigenchannel $\Psi_\alpha$, then the final rotational state distribution $P_j$ is given by $|Y_{j0}(\gamma_0,0)|^2$. Table 2 shows the distributions $P_j$ corresponding to $\gamma_0=0$, $\pi/10$, $\pi/5$, $3\pi/10$, $2\pi/5$, $\pi/2$. If the number of channels participating in the photodissociation are known, the localized angles corresponding to $\Psi_\alpha$ can be obtained by assuming that angles are evenly distributed in the interval $[0, \pi/2]$. The angles shown in Table 2 correspond to 6 channel case. The reason why magnitudes of expansion coefficients shown in Table 2 do not decrease as $j$ increases can be found in the uncertainty relation $\Delta j\Delta\theta\sim h$. The latter relation tells us that $\Delta j\to\infty$ when $\Delta\theta\to 0$. Since angle functions are not sharply localized in angle, the value of $\Delta j$ should be finite. For $r_e$=3.044 a.u. case, Figure 6 shows that $\Delta\theta\sim\pi/10$, which indicates $\Delta j\sim 3$.

**Approximations on $B_\alpha^{-(l)}$ and cancellation between them.** Then $B_{\alpha=1}^{-(nj)}$ may be approximated as

$$B_1^{-(nj)}\approx U_{nj,1}e^{i\mu_1}\Delta_{1,1}+U_{nj,7}e^{i\mu_7}\Delta_{7,1}$$
$$B_7^{-(nj)}\approx U_{nj,1}e^{i\mu_1}\Delta_{1,7}+U_{nj,7}e^{i\mu_7}\Delta_{7,7} \quad (37)$$

Since $U_{nj,1}$ and $U_{nj,7}$ are the frame transformation matrices between the angle function localized around $\gamma=90°$ and the spherical harmonics $Y_{j0}(\gamma, 0)$, they may have similar values, $U_{nj,1}\sim<Y_{j0}(\gamma,0)|\gamma=\pi/2>=Y_{j0}(\pi/2, 0)$. Then $B_1^{-(nj)}\propto U_{nj,1}$. The probability $P_j$ of finding the photofragment having the rotational quantum number $j$ might then be proportional to

$$P_j=[Y_{j0}(\pi/2)]^2=\sqrt{2j+1}\frac{(j-1)!!}{j!!}. \quad (38)$$

Actual calculation yields the final rotational distribution of photofragment different from the above prediction. This derives from the fact that though $U_{nj,1}$ and $U_{nj,7}$ have similar magnitudes as asserted above, their signs are not the same in order for them to be orthonormal as imposed by the unitarity of $U$. In order to satisfy the orthogonality,

$$U_{n=1j,1}\sim U_{n=1j,7}$$
$$U_{n=0j,1}\sim -U_{n=0j,7}. \quad (39)$$

The reason why $U_{nj,\alpha}$ for $\alpha=1$ and 7 have opposite signs for $n=0$ (open) while they have same signs for $n=1$(closed) is that the energy of the open channel wavefunction is higher than that of the closed channel wavefunction. Because of this cancellation, the final state distributions of photofragments depend sensitively on the small terms of $U_{nj,\alpha}$. In other terms, angle functions whose values are localized in different angles from 90° also contribute to the photodissociation dynamics. In case of 12 channel and $r_e$=3.044 a.u., two major terms almost cancel each other, but the uncancelled part is still big enough to form the envelope of the major shape of the final state distribution. The fast oscillating part like the binodal structure is the result of the remaining small terms. For example, in the binodal structure obtained for $r_e$=3.044 a.u., two peaks are located at $j=0$ and 6. The second peak located at $j=6$, owing to which the distribution is tagged binodal, comes from the contribution from $\alpha=6$. This can be confirmed like this. First, the final state distribution obtained by including two major terms $\alpha=1$ and 7 is the monotonically decreasing function of $j$ as shown in Figure 3. Thus the contributions from the two alone can not make the second peak. We found that the second peak is obtained by including $\alpha=6$ term. The $\alpha=6$ term corresponds to the angle function localized around $\gamma\sim\pi/5$ (36°) as can be seen in Figure 6 and 7. Figure 3 shows that $P_j=|Y_{j0}(\gamma, 0)|^2$ has a peak at $j=6$. Rough but easier way of finding $P_j$ for $\alpha=1$ and 6 is to use Table 2 instead of Figure 3.

**Causes and implications of cancellation.** In the above, if the cancellation does not take place, photodissociation rate would be more than 30 times larger than that with

cancellation. Knowing the cause of cancellation may help us find out systems with much greater photodissociation rates and may thus be important. Let us thus examine more on this cancellation. Cancellation occurs for two short-range channels, say $\alpha_1$ and $\alpha_2$ channels whose eigenphases $\pi\mu_\alpha$ (or eigenquantum defects $\mu_\alpha$) are almost equal. Such channels are $\alpha=1$ and 7 for $r_e=3.044$ a.u. and $\alpha=6$ and 8 for $r_e=5.044$ a.u. The designation of channel numbers for $\alpha$ is shown in Figures. 4, 5, 6, and 7, Figure 4 shows that they are almost equal in the neighborhood of resonance energies. As already mentioned above, these two $\alpha$'s are angle functions localized around $\gamma=\pi/2$. Being angle functions implies that in $\Psi_\alpha$, motions in $\gamma$ and $r$ are decoupled and $\Psi_\alpha$ may be approximated as products of wavefunctions of vibrational, rotational, and translational motions.

$$\Psi_\alpha=\sum\Psi_{nj}U_{nj,\alpha}\cos\ \pi\mu_\alpha$$
$$=\sum_{n'j'}\Phi_{n'j'}\sum_{nj}\chi_{n'j',nj}(R)U_{nj,\alpha}\cos\ \pi\mu_\alpha. \quad (40)$$

Since $\chi_{n'j',nj}$ has an asymptotic form of $f_{n'j'}(R)\delta_{n'j',nj}-g_{n'j'}(R)K_{n'j',nj}$, it can be written in the form:

$$\chi_{n'j',nj}(R)=\sum_\beta U_{n'j',\beta\omega}(R)U^t_{\beta nj}, \quad (41)$$

where $\omega(R)$ strictly depends on $n'j'$ but such dependence maybe ignored if we remind that $\alpha$ channel is defined in the short-range where the magnitude of the potential energy is so large that the differences in the kinetic energies for different $(n'j')$'s may be neglected. By substituting this transformation,

$$\Psi_\alpha\approx(\sum_{n'j'}\Phi_{n'j'}U_{n'j',\alpha})\ \omega_\alpha(R)\cos\ \pi\mu_\alpha$$
$$\equiv\Phi_\alpha\omega_\alpha\ \cos\ \pi\mu_\alpha, \quad (42)$$

where the approximation enters when the dependence of $\omega_\alpha(R)$ on $(n'j')$ is ignored. If we assume that $<n=0|\Psi_\alpha>$ and $<n=1|\Psi_\alpha>$ have the same angle dependencies, or, they are localized in the same angle, then the angular part can be separated out from $\Phi_\alpha$:

$$\Phi_\alpha\equiv\sum_{n'j'}\Phi_{n'j'}U_{n'j',\alpha}\approx(a<r|0>+b<r|1>)\sum_{j'}Y_{j'0}(\gamma,\ 0)Y_{0j',\alpha}. \quad (43)$$

$\sum_{j'}Y_{j',0}(\gamma,0)U_{0j',\alpha}$ is just the angle function we said repeatedly before and might be denoted by $\delta(\gamma-\gamma_\alpha)$ if it is a Dirac type function. Actually it is not the type of a Dirac function and has a distribution in $\gamma$. Configuration interaction theory tells us that, in the neighborhood of a resonance energy, only one type of continuum wave functions (or open channel wavefunctions) can inteact with a discrete state consisting of only closed channel wavefunctions. Since the discrete state wavefunction in the current system of A-$B_2$ van der Waals molecule is localized around $\gamma=\pi/2$, a continuum wavefunction localized in $\gamma=\pi/2$ can only interact with the discrete state. The mixing coefficients between discrete and continuum wavefunctions vary rapidly in the neighborhood of a resonance energy. Since $\Psi_\alpha$ is defined from origin up to $R=R_0$ and the rapid variations of mixing coefficients can only occur when boundary conditions at $R\rightarrow\infty$ are applied, the mixing coefficients in Eq. (43) may not vary rapidly as in configuration interaction theory. Numerical calculation shows that mixing coefficients $a$ and $b$ are almost equal. The reason why they are almost equal around resonance is not answered in the current work and remains to be explored. Almost equal mixing between the discrete and the continuum wavefunction implies that two $\mu_\alpha$ corresponding to two mixed states should be almost equal. $\Psi_\alpha$ corresponding to them then take the following form:

$$\Phi_\alpha=\begin{cases}(<r|0>+<r|1>)\sum_{j'}Y_{j'0,\alpha} \text{ for } \alpha=1(6) \text{ and} \\ \quad r_e=3.044\ (5.044) \text{ a.u.,} \\ (<r|0>-<r|1>)\sum_{j'}Y_{j'0}U_{j'0,\alpha} \text{ for } \alpha=7(8) \text{ and for} \\ \quad r_e=3.044\ (5.044) \text{ a.u..}\end{cases} \quad (44)$$

Eq. (44) tells us that, in $\Psi_\alpha$ localized at $\pi/2$, vibrational motion of $B_2$ is also localized either to the left or to the right end of $B_2$. The fact that two $\Psi_\alpha$ are mirror images of each other with respect to $r\rightarrow-r$ ensures that they have almost identical phase shifts. Thus two $\Psi_\alpha$ localized at $\gamma=\pi/2$ correspond to wavefunctions whose vibrational motions are localized at the left and right ends of $B_2$. Photodissociation processes along two $\Psi_\alpha$, which are much larger than the remaining processes, interfere destructively as we saw above. Whether this cancellation is due to the homonuclearity of $B_2$ is remained to be investigated [there are some experiments where A-BC system has a much broader spectral width (faster predissociation) than that for A-$B_2$].[1] Figure 1 tells us that similar cancellation takes place in the IOS approximation, due to the zero of $A(\gamma)$ at 90°. Since $A(\gamma)$ is zero by symmetry with respect to the change of $\gamma$ into 90°-$\gamma$ at 90°, we may expect no such cancellation for the A-BC system. It is an open question, at the present stage, whether two types of cancellation is identical in essence. The further discussion on this topic is beyond the scope of this paper.

**Different interference formula of $B_\alpha^{-(i)}$ shorn of cancellation.** In the IOS analysis, such cancellation is already built in $A(\gamma)$ and we can concentrate on the small terms remaining after cancellation. Similarly, we can also build in the cancellation in the MQDT analysis. Eq. (30) shows us that the summation which causes cancellation in $\sum_\alpha U_{i\alpha}e^{i\pi\mu_\alpha}A_{\alpha\rho}$ yields $T_{i\rho}e^{i\pi\tau_\rho}$. Numerical study confirms that cancellation is done in $T_{i\rho}e^{i\pi\tau_\rho}$. Then instead of using Eq. (33) to calculate $B_\alpha^{-(i)}$, the following equation

$$B_\alpha^{-(i)}=\sum_\rho T_{i\rho}e^{i\pi\tau_\rho}A_{\alpha\rho}, \quad (45)$$

can be used. Eq. (45) explores the effect of interferences among eigenchannels $\rho$ in the asymptotic region on $B_\alpha^{-(i)}$ in comparison with Eq. (33) which explores the effect of interferences among short-range eigenchannels $\alpha$ on $B_\alpha^{-(i)}$. The extent of the contribution of each eigenchannel $\rho$ may be assessed by the time delayed of each eigenchannel $\rho$. Intuitively, more coupling and more contribution will be expected for the eigenchannel $\rho$ where fragments spend more time and are delayed more in coming out of the reaction zone. The amount of time delayed can be estimated by examining the difference between values of short-range eigenquantum defects, namely $\mu_\alpha-\mu_\beta$, where $\mu_\alpha>\mu_\beta$ and no other eigenquantum defect lies between them. This argument is based on the following general properties of $\tau_\rho$. The $\tau_\rho$ becomes $\mu_\alpha$ at off-resonance. Time delayed is proportional to the energy derivative of $\tau_\rho$. If the time delayed is caused by a quasi bound state, it is positive since the quasi bound state will grab photofragments temporally. Therefore, $\tau_\rho$ al-

ways increases as a function of energy in the neighborhood of resonance energy. At off resonance, it should approach one of $\mu_\alpha$. Since there is no symmetry that prevents eigenchannels $\rho$ from interacting each other, $\tau_\rho$ starts from one of $\mu_\alpha$ and it increases dramatically in the neighborhood of resonance energy and then it approaches next higher $\mu_\alpha$. If we restrict the values of $\tau_\rho$ in the range of $[-0.5, 0.5]$, then when the value of $\tau_\rho$ reaches 0.5, its value will shift by minus one and then it will increase to approach the lowest $\mu_\alpha$. This behavior confirm to the general theorem of eigenquantum defect sum $\sum_\rho \tau_\rho$ found by Hazi.[12] The theorem says that eigenquantum defect (eigenphase) sum undergoes a change by 1 ($\pi$) in the neighborhood of resonance energy. The described properties of $\tau_\rho$ is nicely shown in Figure 4.

According to the above argument, $\alpha=3$ channel corresponding to the angle function which is localized around $\gamma=54°$ feels the largest coupling potential for $r_e=3.044$ a.u. For $r_e=5.044$ a.u., Figure 5 shows that the corresponding channel is $\alpha=4$ channel for which the angle function is localized around $\gamma=72°$. Thus the largest contribution to the photodissociation comes from the smaller angle for $r_e=3.044$ a.u. than that for $r_e=5.044$ a.u.. As we said before, the largest torque occurs around $\gamma=60°$. This may be the cause of the binodal structure found for $r_e=3.044$ a.u..

## Conclusion and Discussion

In this work, we focused on the setup of the tools for the analysis of final rotational state distribution. We found that a sort of reflection principle can also be applied to find out the final rotational state distributions for indirect photodissociation processes as in case of direct photodissociation. The analysis is made by first applying Golden-rule like expression to the partial photodissociation cross sections and then by applying IOS approximation to the continuum wave functions in Golden-rule expressions. Applying semiclassical approximation then gives the formula for reflection principle. Here $A(\gamma)$ which is obtained by integrating the product of quasi-bound state, $\partial V/\partial r$, and $\Psi^{IOS}(R|\gamma)$, is reflected into the mirror of the classical angular momentum function, instead of the wavefunction before light absorption. The magnitude of $A(\gamma)$ is the measure of the vibrotational channel coupling strength which brings about the dissociation of van der Waals molecule. The torque $\partial V/\partial\gamma$ which is felt by the diatomic photofragment in the decomposition along the fixed angle $\gamma$ determines the angular momentum with which the diatomic fragment will rotate after dissociation. Figure 1 exhibits the rotational reflection principle diagrammatically.

Setting up the tools of analysis by MQDT is more difficult than that by IOS. Instead of assuming the presence of the quasi bound state wavefunctions, it relies only on the raw concepts like the boundary conditions on channel wavefunctions and couplings among channels in order to explain the resonance phenomena. The strength of MQDT is in the full utilization of the energy sensitive- and insensitive-ness of the dynamic quantities. Such utilization is easily done by making use of the fact that the dynamic coupling occurs at the short-range region, $R<R_o$, where potential energy is highly negative and photon energy variation is much smaller than the modulus of the potential. Thus in MQDT, transition dipole moments are analyzed in terms of those transition dipole moment $D_\alpha$ corresponding to the excitation to $\Psi^\alpha$.

Examination of the short range eigenchannel basis functions reveals that they are angle functions, *i.e.* they are localized around some angle. Two of the angle functions are found to be localized around $\gamma=90°$. According to configuration interaction theory, they correspond to the wavefunctions resulting from the configuration interaction of a quasi bound wavefunction and $\psi_E^{(a)}$, as described in Ref. 6. Two $\Psi_\alpha$'s are found to be not only angularly localized functions in $\gamma=90°$ but also motions along $r$ are also localized at either one of ends of $B_2$. Photodissociation processes along two paths corresponding to two $\alpha$'s dominate over other photodissociation processes but cancel each other. This cancellation causes photodissociation to depend sensitively on the interaction potential at other angles than $\gamma=90°$. Part of potential surface where much larger torque exists can now play an important role in photodissociation. MQDT also enables us to see which processes play important roles after cancellation. This is possible by examining the interference in the eigenchannels at asymptotic region in $B_\alpha^{-(i)}$. The $\mu_\alpha$ *vs.* E graph and the $\tau_\rho$ *vs.* E graph then tell us which eigenchannels are the important contributors to photodissociation.

Since the purpose of this paper is to setup the tools for the analysis of photodissociation process in the neighborhood of resonance region, we have not examine the effects of heterogenuity of diatomic molecules, reduced masses between A and $B_2$, coupling strength and so on on photodissociation. Studies on such effects might be valuable if we take the real system. Application of the analytic methods developed here to real systems are remained to be explored.

**Acknowledgment.** This work was supported by KOSEF under Contract No. 913-0303-001-2.

## References

1. (a) Janda, K. C. *Adv. Chem. Phys.* **1985**, *20*, 201. (b) Buckingham, A. D.; Fowler, P. W.; Hutson, J. M. *Chem. Rev.* **1988**, *88*, 963. (c) Dickinson, A. S.; Lin, W.-K. *Mol. Phys.* **1994**, *82*, 629. (d) Roncero, O.; Villarreal, P.; Delgado-Barrio, G.; Halberstadt, N.; Janda, K. C. *J. Chem. Phys.* **1993**, *99*, 1035.
2. (a) Schinke, R. *J. Phys. Chem.* **1986**, *90*, 1742. (b) Schinke, R.; Engel, V. *Faraday Discuss. Chem. Soc.* **1986**, *82*, paper 11.
3. Fano, U. *Phys. Rev.* **1961**, *124*, 1866.
4. (a) Lee, C. W. *Bull. Korean Chem. Soc.* **1995**, *16*, 850. (b) Combet-Farnoux, F. J. *J. Chem. Phys.* **1982**, *25*, 287.
5. Fano, U. *Phys. Rev.* **1970**, *A2*, 353.
6. (a) Lee, C. W. *Bull. Korean Chem. Soc.* **1991**, *12*, 228. (b) Lee, C. W., *Bull. Korean Chem. Soc.* **1995**, *16*, 957.
7. See Ref. 1(b).
8. Halberstadt, N.; Beswick, J. A.; Janda, K. C. *J. Chem. Phys.* **1987**, *87*, 3966.
9. Child, M. S. *Molecular Collision Theory*; Academic, London, 1974.
10. (a) McGuire, P. *Chem. Phys. Lett.* **1973**, *23*, 575. (b) McGuire, P.; Kouri, D. J. *J. Chem. Phys.* **1974**, *60*, 2488. (c)

Pack, R. T. *J. Chem. Phys.* **1974**, *60*, 633. (d) Schinke, R. *J. Phys. Chem.* **1986**, *90*, 1742.
11. Fano, U.; Rau, A. R. P. *Atomic Collisions and Spectra*; Academic, Orlando, 1986.
12. Hazi, A. U. *Phys. Rev.* **1979**, *A19*, 920.

# Theoretical Studies on the Acyl Transfer Reactions Involving a Tetrahedral Intermediate†

**Doyoung Lee, Chang Kon Kim, Bon-Su Lee, and Ikchoon Lee**

*Department of Chemistry, Inha University, Inchon 402-751, Korea*
*Received August 30, 1995*

Theoretical studies of the effect of the nonleaving group (RY) on the breakdown mechanism of the tetrahedral anionic intermediate, $T^-$, formed by the addition of a less basic phenoxide nucleophile (X) to phenyl benzoates with a more basic phenoxide leaving group (Z) have been carried out using the PM3 MO method. The identity acyl transfer reactions (X=Z) are facilitated by an electron-withdrawing RY whereas they are inhibited by an electron-donating RY group. The results of non-identity acyl transfer reactions indicate that a more electron-donating RY group leads to a greater lowering of the higher barrier, TS2, with a greater degree of bond cleavage, and a greater negative charge development on the phenoxide oxygen atom, whereas the opposite is true for a more electron-withdrawing RY group, *i.e.*, leads to a greater lowering of the lower barrier, TS1. The results provide theoretical basis for the signs of $\rho_{XY}(>0)$ and $\rho_{YZ}(<0)$ observations.

## Introduction

Two distinct reaction pathways have been suggested for nucleophilic substitution at a carbonyl carbon.[1] One step concerted mechanism proceeds through a tetrahedral transition state (TS),[2] whereas two-step addition-elimination processes occur via a tetrahedral intermediate, **I**.[3] In the step-wise pathway, a mechanistic change-over can take place from rate-limiting breakdown to formation of the intermediate depending on (i) relative basicities ($pK_a$) of the nucleophile (NX) and nucleofuge (LZ) and (ii) electron-donating or electron-withdrawing power of the nonleaving group (RY).[3]

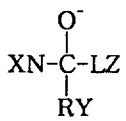

**I**

In a previous work[4] we examined theoretically the effects of relative basicities (or proton affinities) of the nucleophile and nucleofuge on the acyl transfer mechanism using gas-phase reactions of a series of substituted phenoxide anions ($NX=^-OC_6H_4X$) with meta-nitro, para-nitro and 3,4-dinitro phenyl formates ($LZ=OC_6H_4Z$ with $Z=m\text{-}NO_2$, $p\text{-}NO_2$ and $3,4\text{-}(NO_2)_2$ for RY=H). The results suggested that whichever is the lower basicity phenoxide anion the TS level involving partial bond cleavage of that lower basicity phenoxide gives the lower TS. Thus the depression of the TS1 level due

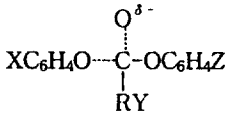

TS1

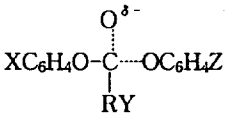

TS2

to a decrease in the basicity of the phenoxide anion nucleophile with a constant nucleofuge may lead to a lower TS1 level than TS2 and the mechanistic change from rate-limiting formation to breakdown of the tetrahedral intermediate, $T^-$, can take place. It was also found that solvation by one water molecule leads to a greater degree of depression of the second barrier, TS2, than that of TS1 and the reaction is expected to change to rate-limiting formation of $T^-$ (or to a concerted process when $T^-$ becomes extremely unstable) as experimentally observed in solution for all the compounds studied.[5]

On the other hand, it has been shown experimentally that as the electron withdrawing power of the nonleaving group in the addition intermediate, RY, is decreased, or conversely as the electron donating power of RY is increased, the higher basicity phenoxide group expulsion is favored *i.e.*, the TS2 is stabilized more than TS1 if $pK_a(Z)>pK_a(X)$.[4]

Since the effect of RY on the degree of bond cleavage in TS1 ($d_1^*$) and TS2 ($d_2^*$) is important in determinig the sign of $\rho_{XY}$ and $\rho_{YZ}$ in Eq. (1),[6,7] which in turn is important as a mechanistic criteria, we decided to study the effect of RY on the mechnism of the acyl transfer reactions involving a tetrahedral intermediate in a greater detail.

†Determination of Reactivity by MO theory. Part 94. Part 93, Lim, W. M.; Kim, W. K.; Jung, H. J.; Lee, I. *Bull. Korean Chem. Soc.*, **1995**, *16*, 252.